1990-06-01

Plasma wave observations during ion gun experiments

Olsen, R.C.; Weddle, L.E.; Roeder, J.L.

Journal Name: Journal of Geophysical Research; (United States); Journal Volume: 95:A6
http://hdl.handle.net/10945/61030

JOURNAL OF GEOPHYSICAL RESEARCH, VOL. 95, NO. A6, PAGES 7759-7771, JUNE 1, 1990

Plasma Wave Observations During Ion Gun Experiments

R. C. OLSEN AND L. E. WEDDLE

Physics Department, Naval Postgraduate School, Monterey, California

J. L. ROEDER

Space Sciences Laboratory, Aerospace Corporation, Los Angeles, California

Experiments in charge control on the AF/NASA P78-2 (SCATHA) satellite were conducted with a plasma/ion source in the inner magnetosphere. These experiments were monitored with plasma wave instruments capable of high temporal and frequency resolution in the 0–6 kHz frequency range. Ion gun experiments revealed two distinct classes of behavior. Nonneutralized ion beam operation at 1 mA, 1 kV resulted in arcing signatures (spiky in time, broad frequency range), coincident with induced satellite potentials of −600 to −900 V. This signature disappeared when the accelerating voltage was switched off or the beam was neutralized (at which time the satellite body approached potentials of a few volts). The signal is attributed to arcing between differentially charged surfaces. An additional feature was noted in the 100-kHz channel of the wave receiver. During emission of dense, low-energy plasma, a signal is generated which may be at the upper hybrid, or plasma frequency for the local plasma.

1. INTRODUCTION

1.1. *Problem of Satellite Charging*

A satellite orbiting in the ionosphere or magnetosphere is essentially a probe in a plasma. It is not surprising, therefore, that a satellite behaves much as a Langmuir probe in a laboratory setting, acquiring a net charge with respect to the ambient plasma. The resulting potential (or potential energy, $q\phi$) is typically comparable to the thermal energy (kT_e) of the plasma. This is not generally a problem at low altitudes, where the thermal energies are low, but at high altitudes it has long been recognized that satellite surfaces can charge many kilovolts negative with respect to the environment, and each other. Such charging has been associated with satellite anomalies and failures [*McPherson et al.*, 1975; *McPherson and Schober*, 1976].

The commonly accepted mechanism for such anomalies is arcing on the satellite surface between differentially charged insulators, with resulting physical damage, or an electromagnetic pulse into the satellite command/control systems [*Koons et al.*, 1988]. This satellite failure mode is the motivation for studies of the processes involved in satellite charging and the methods for controlling the charging, particularly active control techniques.

1.2. *History of Active Experiments*

Charging experiments. A limited number of active satellite charging experiments have been carried out. Experiments with the Applied Technology Satellites (ATS) 4, 5, and 6 offer most of the available data on active charge control at high altitudes [*Hunter et al.*, 1969; *Olsen*, 1985]. At lower altitudes, experiments with the Space Electric Rocket Test (SERT) II payload, designed to test ion engine technology, were conducted at 1000 km altitude, with limited instrumentation [*Kerslake and Finke*, 1975; *Kerslake and Domitz*, 1979]. Rocket experiments, such as the Porcupine ion beam experiment, have provided brief glimpses of the behavior of such systems [*Kintner and Kelley*, 1981, 1982]. More recently, results from the Argon Release Controlled Study (ARCS) experiments have become available [*Kaufmann et al.*, 1989].

Plasma wave observations. ATS satellites, which provide the bulk of our knowledge on the results of active charge control experiments, did not carry plasma wave receivers, so our information is limited in that respect. Information on the effects of ion beam emission are particularly limited. The main experiments in this domain are the Porcupine and ARCS rocket experiments [*Kintner and Kelley*, 1981, 1982; *Moore et al.*, 1982; *Kaufmann et al.*, 1989]. The Porcupine experiment used a 200-eV Xe^+ ion gun, which resulted in production of ion cyclotron, and more generally, lower hybrid waves, in the oxygen-dominated topside ionosphere [*Jones*, 1981; *Kintner and Kelley*, 1983; *Häusler et al.*, 1986].

Higher-frequency phenomena were reported for the Porcupine experiments by *Pottelette et al.* [1984] and *Thiel et al.* [1984]. High-frequency (e.g., MHz) turbulence was observed. The data were interpreted as the result of coupling between Langmuir plasma waves and a lower hybrid drift instability near the beam source. A separate phenomenon which was identified, at large distances, appeared to result from a density minimum in front of the beam, which destabilized electron cyclotron harmonic waves [*Pottelette et al.*, 1984].

The ARCS rockets carried Ar^+ ion guns. These experiments resulted in observations of numerous low-frequency electrostatic emissions, particularly near the lower hybrid frequency [*Walker*, 1986; *Hudson and Roth*, 1984]. The first ARCS experiment was launched on January 26, 1980. The argon beam operated at 100 mA, 25 eV [*Moore et al.*, 1982].

The Ar^+ ion generators were flown again on February 10, 1985, on a sounding rocket launched from Sondre Stromfjord, Greenland, to study ion beam dynamics and ion beam effects on the ionosphere. The generators were arranged

Paper number 89JA03385.
0148-0227/90/89JA-03385$05.00

such that one emitted its beam parallel to the magnetic field, the other perpendicular to the field. During parallel beam operations emissions were observed near multiples of the H^+ cyclotron frequency and the lower hybrid frequency. Perpendicular beam operations produced emissions at He^+ and O^+ cyclotron harmonics [*Erlandson et al.*, 1987].

The noise generated by the discharge itself is of some pertinence. Signals with wavelengths comparable to the size of the discharge chamber will be stimulated. *Kudo et al.* [1983] report observations of discharge noise characteristics in the laboratory for a 5-cm thruster (apparently using Mercury ions). They indicate a variety of coherent peaks, depending on operating mode, at least some of which are interpreted as two-stream instability generated ion-acoustic waves.

There have been limited reports on the ion and electron gun experiments conducted on the SCATHA satellite [*Koons and Cohen*, 1982]. It was found that electrical discharges and arc-generated pulses could be observed during high voltage electron gun experiments (e.g., 1.5 kV, 6 mA). Similar arcing signatures were observed during nonneutral ion beam experiments. The purpose of this article is to extend this earlier work, based on a survey of the complete data set [*Weddle*, 1987].

1.3. *Theoretical Expectations*

A limited number of theoretical calculations have been done for such ion beam experiments. They predict that the hydrogen cyclotron harmonics and the upper and lower hybrid frequencies should be observed [*Kintner and Kelley*, 1983; *Walker*, 1986; *Hudson and Roth*, 1984; *Haerendel and Sagdeev*, 1981; *Roth et al.*, 1983].

Earlier experiments which were the topic of these theoretical treatments took place in the ionosphere where H^+ is a minor constituent. At geosynchronous orbit the environment is mostly H^+ with O^+ ranging from 10 to 50%, and the beam density is large compared to the ambient. The magnetic energy density relative to the plasma energy density (β) is also different in the two regions. While these differences prevent us from applying the results of these calculations to our situation, they do give us ideas on where to start looking. We believe it is reasonable to assume that plasma waves at some frequency would be generated by the SCATHA ion gun. At the SCATHA orbital altitudes, the H^+ cyclotron frequency and the lower hybrid frequency are too low to be observed by the SC1 experiment, although a second receiver (SC10) is occasionally available for this lower-frequency regime. The electron cyclotron frequency was generally a few kilohertz. The majority of the work which follows deals with this higher-frequency range. Unfortunately, the plasma frequency and upper hybrid resonance frequency are not generally within the wideband receiver frequency range.

1.4. *The SCATHA Program*

P78-2 satellite. The Air Force P78-2 satellite was launched on January 30, 1979, as part of the joint NASA/Air Force program on Spacecraft Charging at High Altitudes (SCATHA) [*Fennell*, 1982]. The satellite was placed in a near geosynchronous orbit, at 7.9° inclination, 5.3 R_E perigee, and 7.8 R_E apogee. The satellite was spin stabilized, with a rotational period of about 59 s. The spin axis was oriented perpendicular to the Earth-Sun line, roughly in the orbital plane. Hence, at local midnight, the spin axis was pointing east. The cylindrically shaped satellite measured roughly 1.7 m in diameter and 1.75 m in length. The surface was made up of both insulated and conducting materials. The sides were primarily insulating solar cell glass covers. The satellite was instrumented with an abundance of instruments designed to observe charging effects [*McPherson and Schober*, 1976; *Fennell*, 1982]. In addition, it carried two active charge control experiments and a plasma wave receiver.

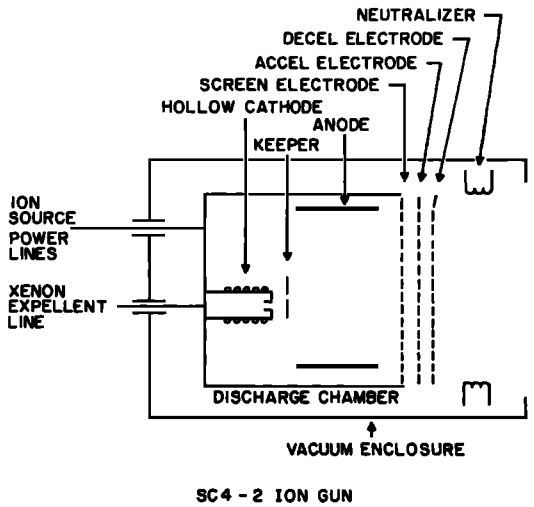

Fig. 1. Ion gun block diagram.

Xenon ion gun. An ion source, designated SC4-2, was provided to emit neutralized and nonneutral beams, at energies of 1 and 2 kV, at nominal currents of 0.3, 1.0, and 2.0 mA. Xenon propellant was utilized in the hollow cathode based system [*Masek and Cohen*, 1978]. The beam neutralization was provided by filament neutralizers, which could be biased in voltage and set at fixed current levels. Since the filament current was not allowed to float, there was generally a small imbalance in the emitted currents, in the beam neutralized mode. This resulted in nonzero satellite potentials observed during such operations. A few essential features of the source are further illustrated in Figure 1. The hollow cathode source inside the chamber had a separate "keeper" anode, which was generally used to start the discharge inside the chamber. The main discharge then was struck to the anode rings along the walls of the discharge chamber. The plasma was extracted by applying high voltage to the grids. With no voltage applied to the grids, but full power to the discharge, a low-current, low-energy plasma could be emitted. This mode was termed "trickle" mode. The charging results from SC4-2 experiments have been studied by *Werner* [1988].

Detectors: SC-1/SC-10. The plasma wave receiver (SC1-8) had two operational elements of interest. The receiver could be connected to the long electric antennas (SC-10), which were 100 m tip-to-tip, or to the air-core magnetic loop antenna. The magnetic loop is on a 2-m boom, with an effective area of 575 m^2 at 1.3 kHz. The magnetic receiver has a sensitivity of 3×10^{-6} nT/Hz$^{1/2}$ at 1.3 kHz and a 60-dB dynamic range. Each of the electric antennas are insulated for the first 30 m of length, then are exposed for the

remaining 20 m. The electric field receiver has a sensitivity of 5×10^{-7} V/m $Hz^{1/2}$ and a set of 8 filter channels with bandwidth ±7.5%, at frequencies of 0.4, 1.3, 2.3, 3.0, 10.5, 30, 100, and 300 kHz. Only the filter data are routinely available. Experiments described below were selected for the availability of wideband data. A lower-frequency wideband channel (0–400 Hz) is available from the SC-10 and SC-11 (magnetometer) experiments, when SC1-8 is in the 0–3 kHz mode. Unfortunately, the 0–400 Hz wideband data were not originally considered, and the tapes were unreadable when we attempted to reprocess the data for the low-frequency wideband range. Four lower-frequency channels are filtered from the SC-10 and SC-11 measurements, at 0.1–1.0, 1.0–2.0, 2.0–20.0, and 20.0–200.0 Hz.

2. OBSERVATIONS

2.1. *Introduction*

Early analysis of the plasma wave data during ion gun operations generally showed signatures which were consistent with pulses generated by arcing [*Koons and Cohen*, 1982]. There was some ambiguity in the data, as to whether the arcing was internal to the ion gun or external. Considerations presented below have indicated that the arcing is occurring on the satellite skin, that is, between differentially charged insulating surfaces or between the insulators and the satellite body.

Three ion gun modes were studied. First, the primary mode for satellite charge control is with both the ion beam and neutralizer on. The satellite is thus emitting a neutralized ion beam. Next, induced (negative) charging experiments were conducted with the ion beam on and the neutralizer off. Only xenon ions are emitted in this mode. Finally, in trickle mode the ion beam discharge is on, but without an accelerating voltage on the grids. Data taken in each of these three modes will be presented.

2.2. *Day 200, 2214–2314 UT*

The first plasma wave observations presented here are from a sequence of ion gun experiments on July 19, 1979 (day 200). These data illustrate typical observations for gun off; gun and high voltage on, neutralizer off; gun on, high voltage and neutralizer off (trickle mode). The satellite location is near local dusk (1954–2042 LT), between $L = 7.6$ and 8.0. The electron cyclotron frequency varies from 1.8 to 2.2 kHz. The hydrogen cyclotron frequency is around 1 Hz, and the lower hybrid frequency is about 40–50 Hz, and hence these latter two fundamental frequencies are off scale.

The plasma wave (wideband) data set presented below began while the ion gun was on with an accelerating voltage of 1 kV and a nominal beam current of 2.0 mA. The neutralizer filament power was off. The satellite was in the dusk bulge region, in a relatively quiet plasma sheet environment. The mainframe was uncharged ($< \pm 10$ V) when the gun was off and charged to approximately −800 V when the gun was on, in the nonneutralized mode.

The operation is summarized in Figure 2. Figure 2 presents the narrowband filter data for the period 2130–2330 UT for both antennas. The ion gun experiments begin at 2130 (system power on) and end at 2300 UT. The 20–30 dB increases in (electric) amplitude at 400 Hz, 1.3 kHz, 2.3 kHz, and 3.0 kHz correspond to operation of the nonneutralized ion beam. Drops in amplitude at 2200 and 2230 occur at times when the accelerating voltage is switched off, sending the gun into trickle mode. Charging analysis shows that the 1-kV beam charged the satellite to potentials of −600 to −800 V when the high voltage was on. Trickle mode results in near-zero voltages [*Werner*, 1988].

The data presented in Figure 2 are heavily processed and smoothed. Figure 3 shows the "raw" data for the 400-Hz and 100-kHz channels, with the electric antenna in the top two panels. The substantial fluctuations in the data are typical of the other channels.

The magnetic field data (Figure 2) show that at 400 Hz the amplitude increase is greater than 40 dB and the signal peaks off the scale (at ~15 dB). The 1.3–3.0 kHz channels show magnetic field amplitude increases of 35–40 dB. During trickle mode the magnetic field amplitudes show a decrease but remain 15–30 dB above background. We interpret the trickle mode data as showing that no interference generated at these lower frequencies reaches the electric antenna but that an electrostatic or electromagnetic signal is caused by the interaction of the "dense" xenon plasma from the gun with the ambient plasma in the immediate vicinity (a few meters) of the satellite, and this signal is observed by the magnetic loop antenna. In contrast to the low-frequency observations, the 100-kHz electric field channel (Figure 3) shows an increase in signal strength during trickle mode. Note that the fluctuations in the 100-kHz signal are minimal, during trickle mode, compared to the HV on data.

Two of the lower-frequency filtered outputs from the quasi-static electric field and magnetometer experiments are presented in the lower half of Figure 3. The vertical axis is telemetered voltage, which has a peak of 5.1 V. The electric field data (thin, solid line) in the three lowest channels are all similar to the 2–20 Hz data (bottom panel). The receiver nearly saturates with the gun on. The magnetometer data from the axis parallel to the spin axis (solid dots) do not show any correlation to the gun operations in the three lowest-frequency channels. The 20–200 Hz magnetic channel shows a substantial response during trickle mode (2230 UT) and again at gun off (~2300 UT). The response at ~2300 UT corresponds to a decrease in the beam current setting to 0.3 mA, just prior to turning the gun off. The difference in magnetometer (SC-11, 20–200 Hz) and search coil (SC1-8, 400 Hz) behavior suggests that the search coil response is due to the electrostatic coupling of the search coil to the electric field emissions. The magnetometer is not susceptible to this type of artifact. The search coil data are therefore interpreted as the near-field (2 m from spacecraft) electrostatic measurements, to be contrasted with the far-field data from the long electric antenna (25-m average).

The details of the plasma wave observations are addressed by means of the wideband data. The wideband data are presented in spectrogram and line plot formats. Typical "gun-off" data are shown in line plot form in Figure 4. The July 19, 1979, broadband data were taken with the plasma wave receiver in the 0–3 kHz mode.

Figure 4*a* shows a frequency spectrum of the magnetic field data with the gun off taken at 2302:59. Three second averages were used to create the frequency spectra presented here. There are monochromatic signals at 700 and 2100 Hz, along with a broad background spectrum peaked at 1 kHz. These monochromatic signals are caused by a 700-Hz tuning-fork driver circuit in another experiment and are not

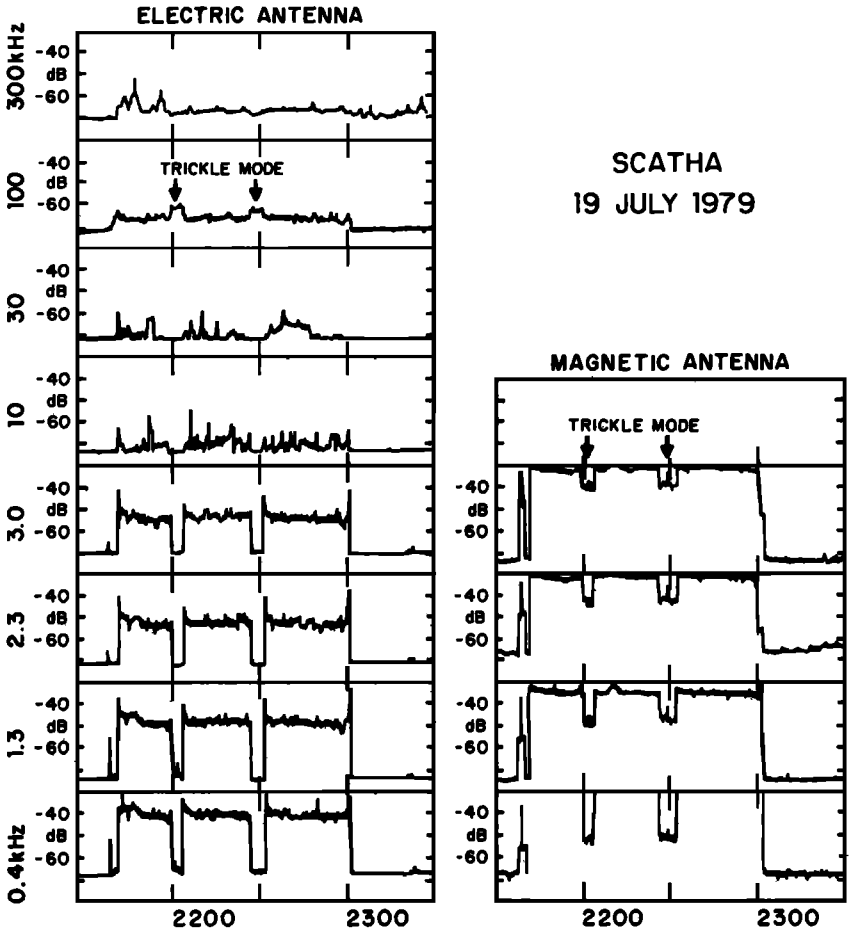

Fig. 2. Plasma wave intensities, day 200.

seen in the electric field data. The broad peak is the resonant response of the receiver to a white noise input, as determined by ground calibration. This noise is not visible in the electric field (E) data. Figure 4*b* shows the frequency spectrum for the electric field data with the gun off taken at 2303:05. Two peaks are found at 2570 and 3155 Hz. At least one of the signals is probably the electron cyclotron harmonic, or $(3/2)f_{ce}$ [*Koons et al.*, 1987]. The low-frequency peak (about 100 Hz) may be an artifact generated on or near the spacecraft. A substantial study of this phenomenon by H. C. Koons and R. Holzworth (private communications, 1987) was unable to resolve this point. If natural, it is a previously unreported feature of magnetospheric plasma wave morphology. It is near the low-frequency cutoff of the receiver band pass [*Koons and Cohen*, 1982].

The nonneutralized, 1-kV, 2.0-mA beam experiment is presented next. Data are shown at 2218 UT, in the middle of the second induced charging sequence. The satellite potential is ~−800 V. Figure 5*a* is a spectrogram showing 46 s of plasma wave for this ion gun operating mode. The horizontal axis is time in seconds, the vertical axis is frequency. All the spectrograms shown here utilize a 0 to 4.0 kHz frequency scale. Signal strength is indicated using a grey scale, with white for low amplitude, black for high. The bandwidth in this mode introduces a roll-off at 3 kHz, as seen in the spectrogram. The plasma wave receiver on the satellite switches antennas every 16 s cycling between the electric

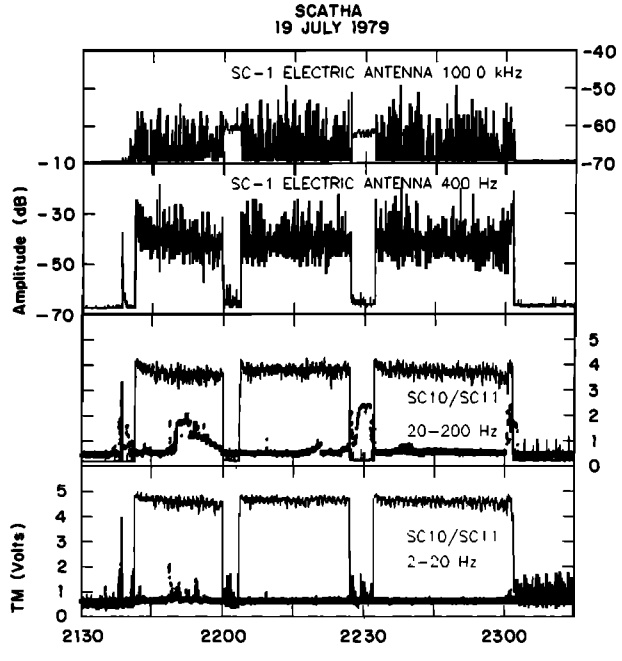

Fig. 3. Detailed plot of SC1 and SC10/11 plasma wave data. The top two panels show the 100-kHz and 400-Hz electric antenna data. The bottom two panels show the SC10/11 data. The electric field (SC10) data are plotted as a thin line. The magnetometer (SC11) data are plotted as dots and generally lie below the SC10 data.

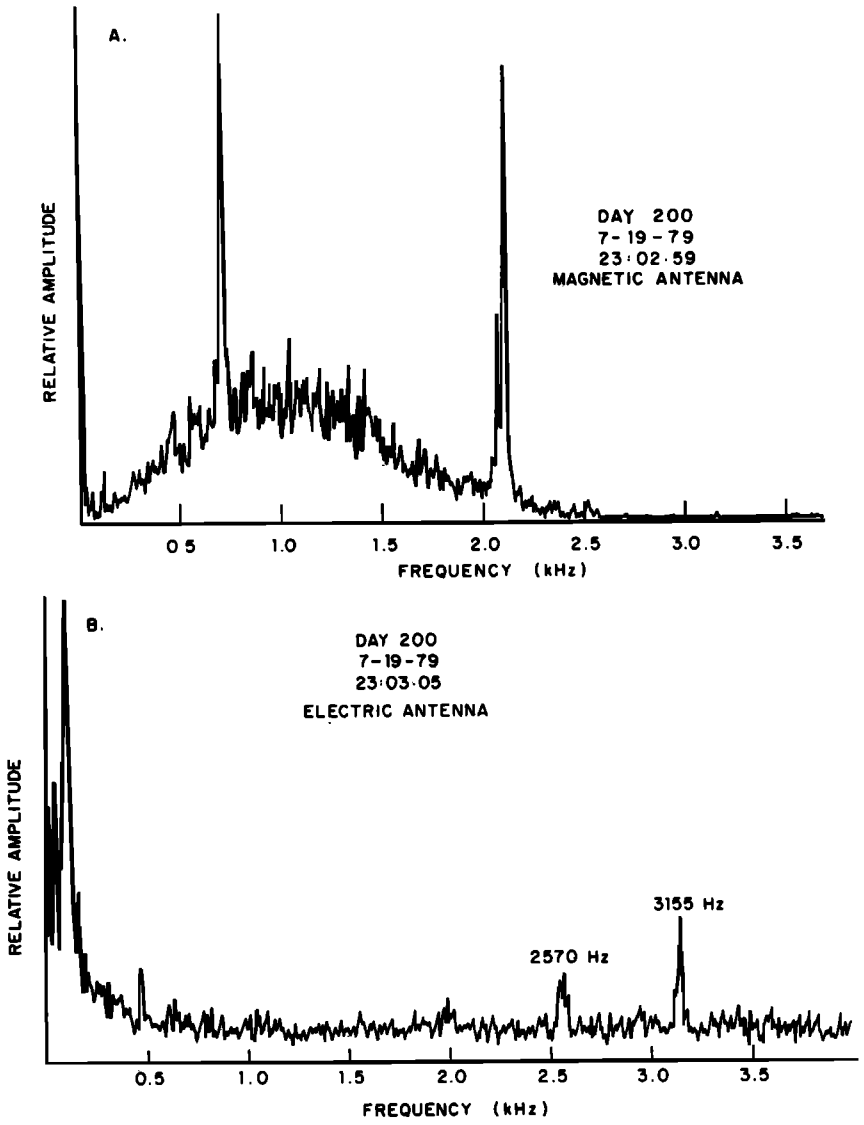

Fig. 4. (*a*) Magnetic loop antenna spectrum, gun off, 2302:59 UT. (*b*) Electric antenna spectrum, gun off, 2303:05 UT.

field antenna and the magnetic field antenna. Hence the spectrograms cycle between the electric field data and the magnetic field data every 16 s. This spectrogram shows the receiver background noise normally present in the magnetic field (*B*) data. Again, the selected antenna was switched every 16 s and the roll-off at 3 kHz is due to the receiver mode. There is a broad maximum from 1.0 to 1.5 kHz visible in the magnetic field data as shown by the darkening of the spectrogram at those frequencies. This signal is not present in the electric field data. Brief, vertical striations in the data, particularly the magnetic data, show a broad spectrum which we interpret as the signal generated by arcing on or in the satellite. The vertical striations are obviously due to pulses with periods considerably less than a second. Indeed, since the frequency spectrum extends to kilohertz, the duration of the pulses is of the order of milliseconds or less.

The frequency spectrum is analyzed in more detail in the following two figures. Figure 6*a* is a frequency spectrum of the magnetic field data at 2218. The spiky aspects attributed to arcing have largely been averaged out by 3-s averaging. Figure 6*a* shows that the most intense average signals are below 500 Hz, followed by a broad peak from 1.1 to 1.4 kHz. This latter peak is the broad maximum visible in the spectrogram and is similar to the receiver noise signal shown in Figure 4*a*. Consideration of calibrated filter data (Figure 2) show that this signal is orders of magnitude higher in amplitude than background noise. This appears to be, therefore, the system response to an intense white noise input signal. Figure 6*b* shows the frequency spectrum of the electric field data at 2218:15. A broad signal, from near zero to about 1.5 kHz, monotonically decreasing in amplitude is found in Figure 6*b* that was not present in the gun-off data of Figure 4*b*. The smaller peaks near 2.5 and 3.1 kHz are still visible. Hence the ambient signal persists, or a similar resonance is being driven. The low-frequency spectrum is similar to that found in the magnetic field data of Figure 6*a*, but there is not a corresponding signal in the 1.0–1.4 kHz range of the electric field spectrum. The small peak at 3.1 kHz is again thought to be the $(3/2)f_{ce}$ signal (f_{ce} = 2.1 kHz at this time).

At 2226:55 the high voltage is turned off resulting in trickle mode. A net ion current of 20–50 μA is still being emitted

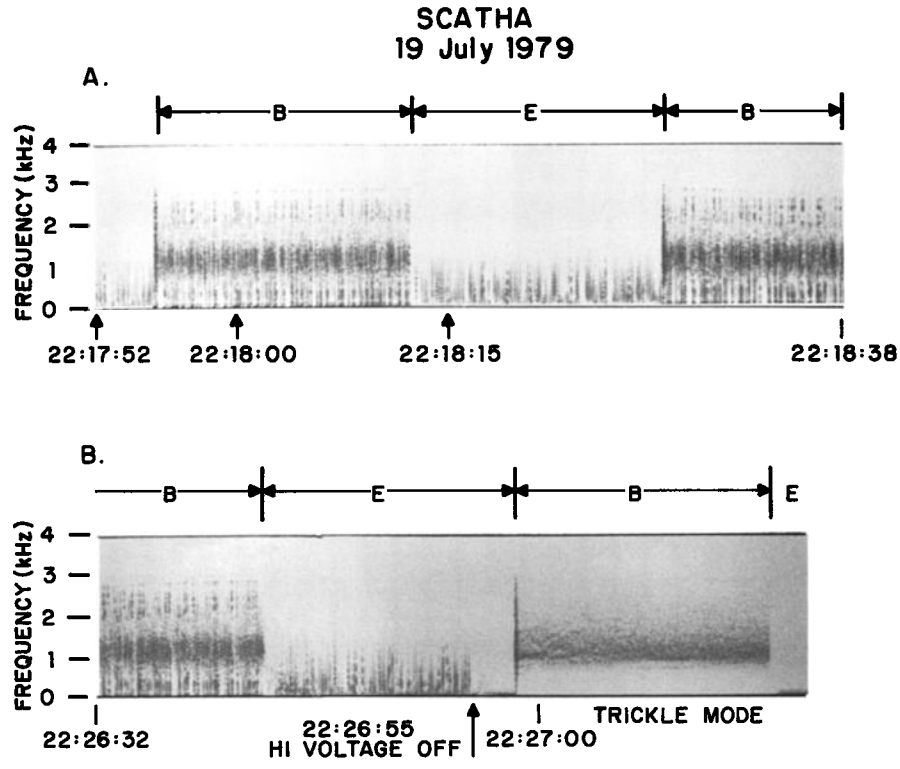

Fig. 5. (*a*) Plasma wave spectrogram for day 200. Gun on, HV on, 1 kV, gun current is 2 mA. Neutralizer is off. (*b*) HV off at 2226:55, ion gun goes into trickle mode.

(according to gun diagnostics). The result of this ion emission is a satellite potential near zero ($<\pm 10$ V). The arcing response seen in Figure 5*a* ceases during an electric field measurement as shown by Figure 5*b*. As previously noted (Figure 3), the electric narrowband channels from 0.1 Hz to 3.0 kHz drop to background, but there is an enhancement at 100 kHz. The 400 Hz to 3.0 kHz magnetic field channels show a decrease, but the signals are well above the "gun-off" values.

Figure 5*b* shows that the broad maximum from 1.0 to 1.5 kHz is still present during trickle mode in the magnetic data while the electric field spectrum no longer shows the 0–1 kHz signal. The signals become cleaner over the next few minutes. By 2229 both the broadband signal in the magnetic field data and the very low frequency signal in the electric field data have become more intense but have not substantially changed in character. The 3.2-kHz signal in the electric field data persists. Figure 7 is a frequency spectrum for the magnetic field data at 2229:45. The broad peak from 1.0 to 1.5 kHz is similar to that found previously, that is, similar to the receiver resonance response to a white noise input. The lower-frequency peak (below 500 Hz) seen in Figure 6*a* is now gone.

At 2232:03 (not shown) the high voltage is turned back on. The arcing resumes, and the data resume their former character. The signals do appear more intense in the spectrogram, but this is probably an artifact of automatic gain control (AGC) and processing variations. This change in the data could reflect different characteristics of differential charging following the trickle mode induced discharge of the dielectric materials [*Olsen*, 1985; *Werner*, 1988].

There are changes in the data which are independent of gun status change. One to two minutes after each trickle mode operation, the amplitude of the waves seen with high voltage on drop by 5–10 dB as visible in Figure 2, for the electric channels. The spectrum is largely unchanged, however.

Changes in the gun current resulted in changes in the wave data. Figures 8 and 9 show the results of decreasing the gun current, just prior to the end of the gun experiments on this day. Figure 8*a* shows the wideband data while the gun is in its 2-mA mode (nominal current is 1.7 mA at this time). The main features, seen previously, are the broadband signal peaking near 1 kHz in the magnetic channel, a lower-frequency broadband signal in the electric channel, and numerous vertical striations which appear to indicate arcing. The beam current is reduced to 1.0 ma at 2258:06, during a "B" sample period. There are no immediately obvious effects in the spectrogram nor in the narrowband data (Figure 9). Within the next minute, however, it becomes apparent that the frequency of occurrence of the striations has decreased. This is illustrated in Figure 8*b* and is most obvious in the magnetic data at 2300:10. The beam current is further reduced at 2300:22, to 0.3 mA, during an "E" sample period (Figure 8*c*). The immediate results are not obvious, but the subsequent "B" sample clearly indicates substantially fewer striations. Fifty seconds later (2301:10), the magnetic data are almost free of the arcing signature (Figure 8*d*), as are the subsequent electric antenna data. The gun is switched off at 2301:40, during a "B" sample, and the broadband data drop to background.

The narrowband data at 1.3 kHz are shown in Figure 9, along with the 20–200 Hz channel of the SC10 and SC11 instruments. The 1.3-kHz channel is typical of the four

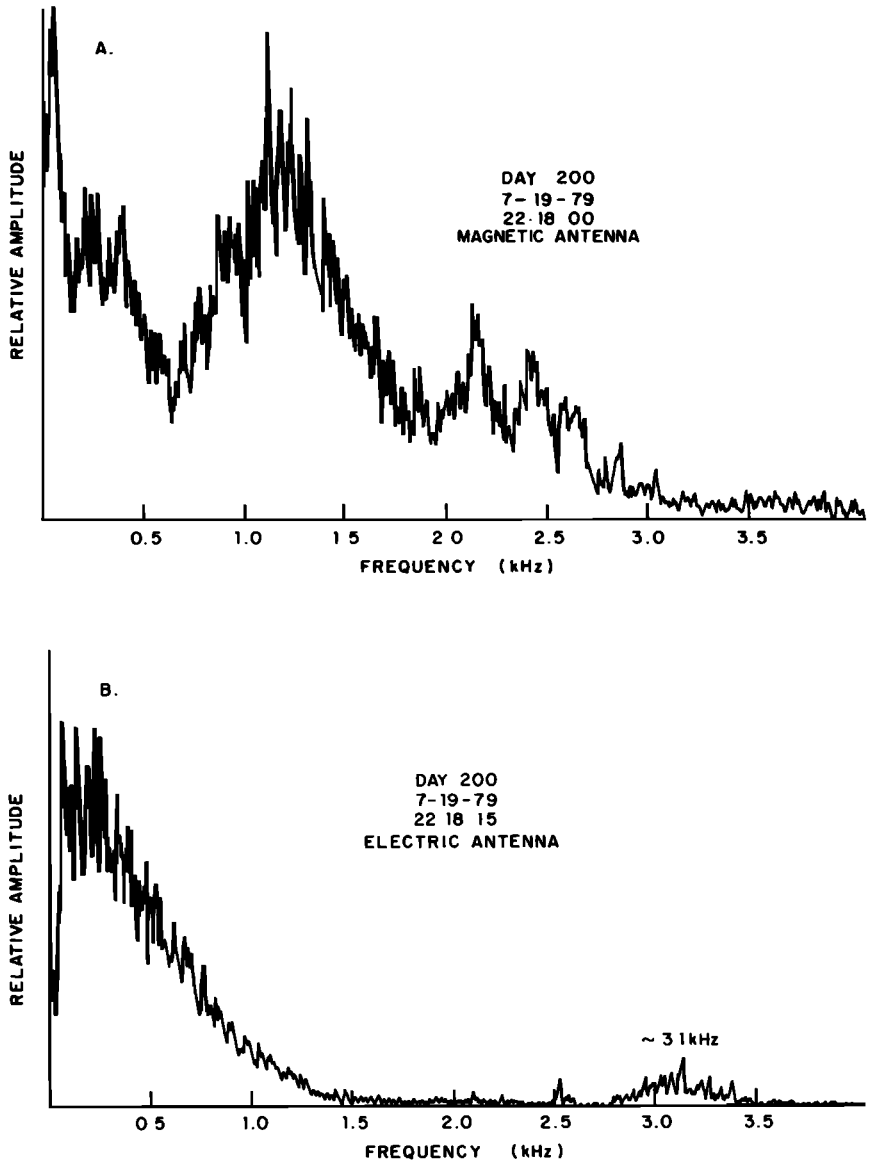

Fig. 6. (*a*) Magnetic loop antenna spectrum, gun on, HV on (1 kV). (*b*) Electric antenna spectrum, gun on.

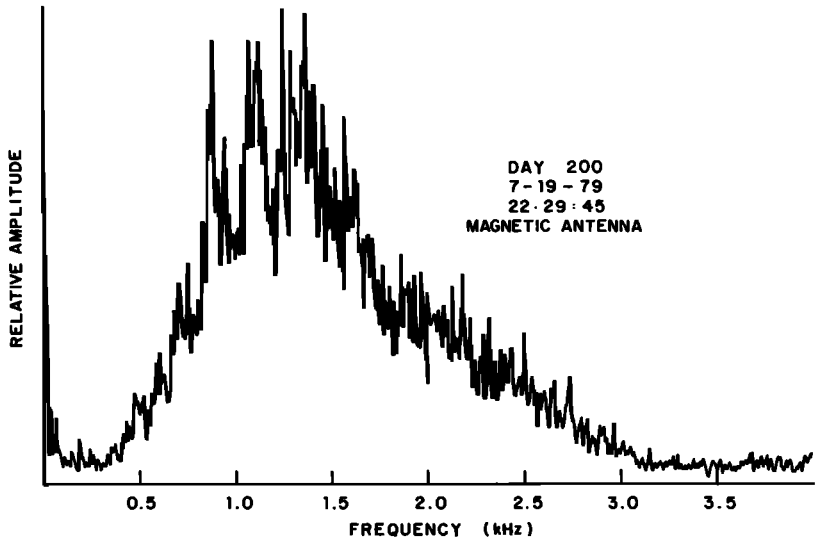

Fig. 7. Magnetic antenna spectrum, day 200, HV off (trickle mode).

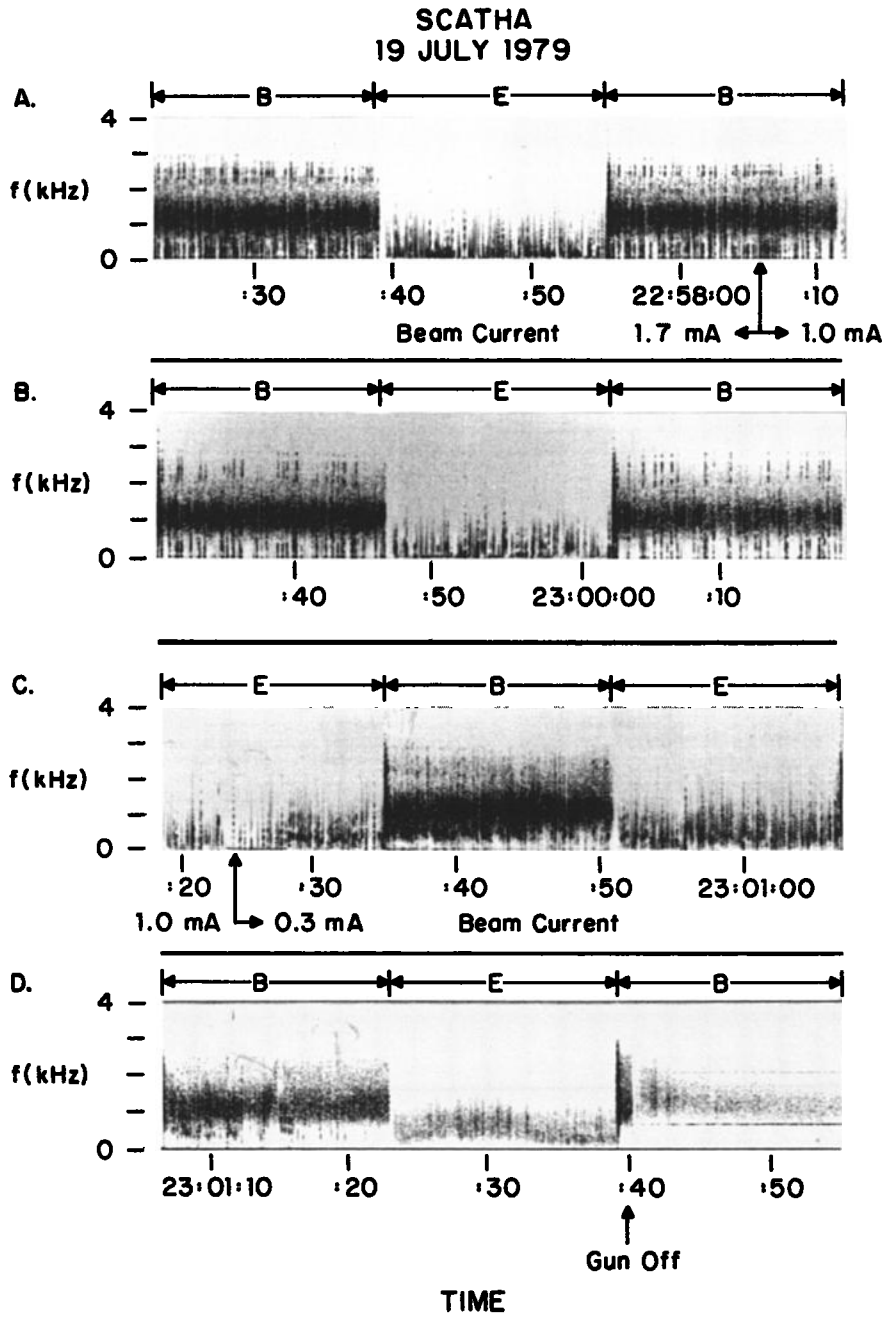

Fig. 8. Plasma wave spectrograms for day 200. Segments in Figures 8*b*, 8*c*, and 8*d* are sequential in time.

lower-frequency SC1 channels during this time segment and was chosen as corresponding to the apparent peak of the magnetic wideband channel. The SC10/SC11 plot is simply an expansion of the latter portion of Figure 3. These data indicate that there is little change in the signals in either receiver when the current is dropped to 1.0 mA (bottom panel). A substantial change is found at 0.3 mA. The 1.3-kHz magnetic antenna amplitude increases by about 10 dB, the electric antenna amplitude by some 20 dB. The increase in the SC10 (electric) antenna response is modest, but noticeable. The magnetometer response (SC11) is substantial, as previously noted in the discussion of Figure 3.

Note that these changes do not arise from a cessation of satellite charging. Since the beam current is ~1 order of magnitude greater than necessary to induce a kilovolt potential, beam limiting mechanisms are at work. One mechanism which would give this effect is the buildup of space charge outside the gun aperture, causing the beam to stall. Only a few percent of the emitted ions escape. The 0.3-mA beam produces a lower ion density (for constant voltage, or ion velocity). The result in general is a more negative satellite potential, indicating more ions escape. Indeed, the satellite potential apparently drops from about −800 V at 1.7-mA beam current, to −900 V to −1 kV at 0.3-mA beam current [*Werner*, 1988].

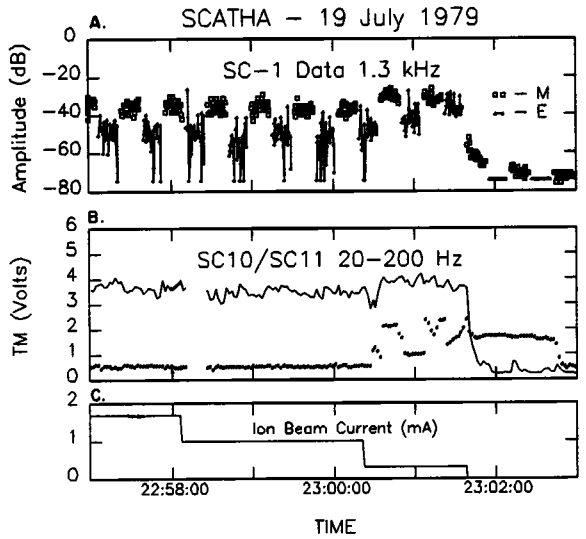

Fig. 9. Plasma wave data for day 200, as the gun current is reduced to zero.

2.3. *April 2, 1979, 1513–1548 UT*

The second operation to be presented occurs in eclipse on day 92 of 1979. Plasma wave response to gun operations appear similar to those observed in the dusk bulge region on day 200. This example extends those shown previously by including the effect of beam neutralization. Beam neutralization prevents substantial induced satellite charging by the ion beam, and hence, arcing on the surface. During this period, the satellite is between $L = 7.3$ and 7.6, just after local midnight. The satellite is in eclipse from 1430:00 to 1537:53. The electron cyclotron frequency varies from 3.2 to 3.6 kHz, the hydrogen cyclotron frequency is about 2 Hz, and the lower hybrid frequency varies from 75 to 85 Hz. Only the spectrograms (Figure 10) and narrowband data (Figure 11) for this period are shown. Attempts to generate amplitude plots for the frequency spectrum were not successful because of the age of the magnetic tape on which the data were stored. The data for this period were taken in the 0–5 kHz receiver mode but are shown only from 0 to 4 kHz. There is no receiver roll-off at 3 kHz in these data.

The data presented next begin with the ion beam on with beam voltage at 1 kV. The beam current and neutralizer current were set at 1 mA (nominal), with the neutralizer biased −10 V with respect to the ion gun. Net current measurements from the gun indicate a net current of about 100 μA. Charged particle data are confused during this period, partly due to rapid and frequent ion gun mode changes. Indications are that on this day, the neutralized beam resulted in potentials of −100 to −200 V, depending on the neutralizer setting. Figure 10*a* shows that there is a diffuse spectrum in both the electric and magnetic field data. In the magnetic channel there is a continuous band of signals from just below 1 kHz to the top of the spectrogram at 4 kHz with the 1–2 kHz region showing slightly greater signal strength. The 700 and 2100 Hz interference lines are not visible. A faint spectrum exists in the electric field data from

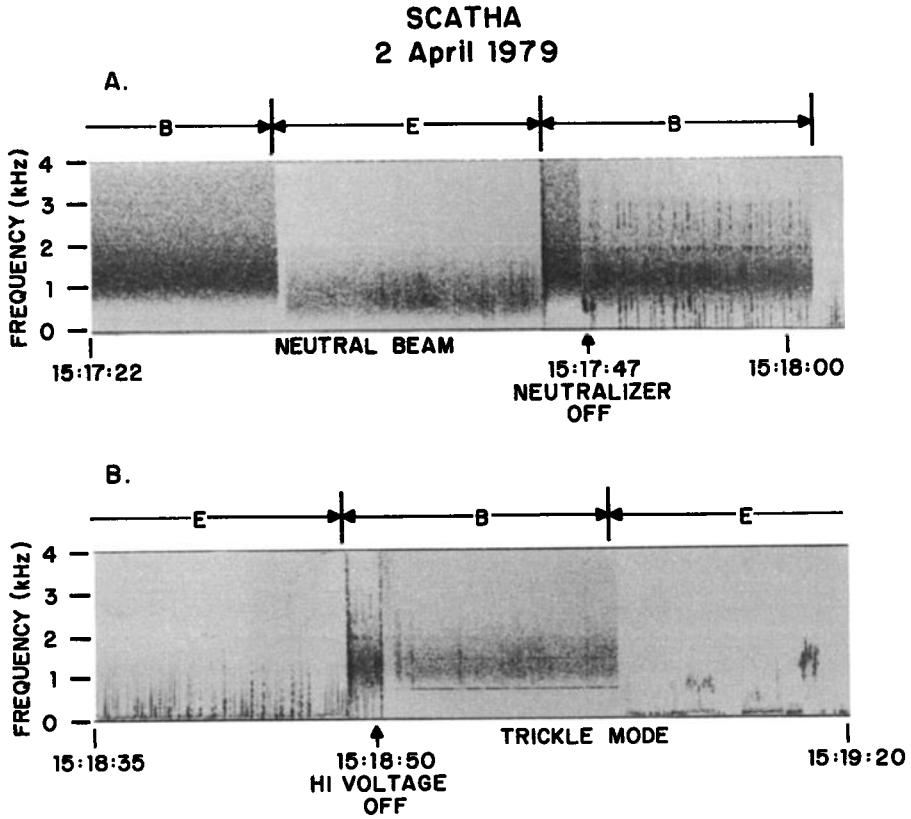

Fig. 10. (*a*) Plasma wave data, wideband, day 92. Neutralized ion beam, 1 kV ions, 1.0-mA beam, 1.2-A neutralizer current. Neutralizer bias is −100 V. Neutralizer off at 1517:47. (*b*) Plasma wave data, wideband, day 92. Nonneutral beam at 1 kV, 1.0 mA initially. HV off at 1518:50.

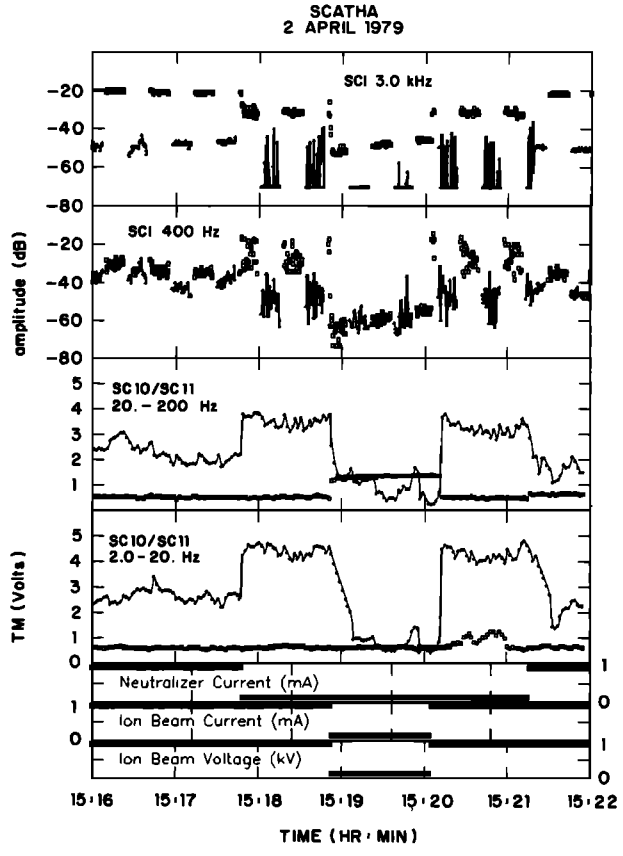

Fig. 11. (Top two panels) Plasma wave data from SC1, 400 Hz, 3.0 kHz. The magnetic field data are shown with small boxes, the electric field data with dots and lines. Note the alternation in antenna at 16 s intervals. (Middle two panels) SC10/11 data at 2.0–20.0 and 20.0–200 Hz. Solid lines are electric antenna (SC10), boxes are magnetometer data (SC11). (Bottom three panels) The gun parameter settings.

0.4 to 1.5 kHz. This diffuse spectrum is regularly seen during such neutralized beam operations. Examination of filter data (presented below) show that this signal amplitude has increased relative to the trickle mode data.

Figure 10*a* shows how the data change with the neutralizer off (neutralizer off at 1517:47). The neutralizer off data resembles the data from day 200 at similar gun settings. The broad frequency spikes and the intense 1.0–1.5 kHz band are both present in the magnetic field data. The electric field data appear similar to the arcing data shown for day 200. Figure 10*b* shows data taken as the high voltage is turned off at 1518:50. The gun enters trickle mode at that point. The emitted current is 10–50 μA. Visible at this time in the magnetic field data are the 700-, 1400-, and 2100-Hz interference lines and the diffuse background noise. The electric field data contains a very low frequency (less than 100 Hz) signal and some spotty signals near 1 kHz.

These data demonstrate that the "arcing" behavior is external to the ion gun, since the gun voltages are all on for the neutralized beam experiments. The absence of arcing during trickle mode, as well, shows the spiky behavior in the wideband data must correspond to arcing on the satellite surface.

Figure 11 shows the electric and magnetic field amplitudes corresponding to these spectra. The 16-s antenna cycling pattern is apparent here, as in the spectrograms. The 3-kHz and 400-Hz data are shown in the top two panels and are representative of the other channels. The nominal beam and neutralizer settings are plotted below. Note that there is an imbalance in the emitted currents of 10–100 μA (e.g., a few percent), which results in net negative charging. The neutralized beam (approximately first 2 min) results in a relatively high noise level in the 3-kHz magnetic loop (small boxes). The 3-kHz noise level drops when the neutralizer is switched off and the amplitude drops again when the beam voltage is switched off. The sequence is inverted as the beam voltage is switched on, and then the neutralizer. The behavior of the 400-Hz data differ, in that the highest noise level occurs for the beam on, but neutralizer off. This corresponds to the arcing period. The electric channel only responds at the lower frequencies, with virtually zero response above 3.0 kHz. There was not a 100-kHz response during trickle mode, in contrast to observations on July 19, 1979 (Figure 3).

Finally, Figure 11 shows the SC10 and SC11 data in the bottom two panels. The SC10/11 data are recorded for 0.1–1.0 Hz, 1.0–2.0 Hz, 2.0–20.0 Hz, and 20–200 Hz. Data are shown for the 2–20 Hz and 20–200 Hz channels. The solid line (with dots) shows the electric antenna data, the small boxes are the magnetometer data. At low frequencies (0.1–20 Hz), little or no signal is found in the magnetic field data. The electric channels are near zero (background) during trickle mode. In the 20–200 Hz data, slightly different behavior is found. The magnetometer data show a sharp increase during trickle mode, and the electric data remain above background. This increase in the 20–200 Hz magnetometer output is similar to that shown for July 19, 1979. The electric channel 20–200 Hz response is larger and is spin modulated.

2.4. *Summary of Observations and Analysis*

Broadband and narrowband wave data taken during the ion gun operations conducted throughout 1979 were surveyed. Data presented above were chosen to show typical responses observed in the complete survey. Plasma wave response to ion gun operations showed little dependence on satellite location within the magnetosphere, or environmental considerations.

The major feature which was observed in the magnetic antenna data, for trickle mode, neutralized beams, and nonneutralized beams, was a broad peak from 1.0 to 1.5 kHz which represents the white noise response of the receiver (Figures 5, 6*a*, 7, and 8*a*). The common feature in these cases is the mixture of a relatively cold, dense plasma with hot, tenuous plasma. (Also, the dense plasma is spatially limited.) The apparent current dependence of the broad peak (Figure 9) is presumably tied to the change in beam-limiting processes. It may be that space charge oscillations outside the beam aperture are one source of the observed broadband signals.

The nonneutralized beam experiments result in satellite potentials approaching a kilovolt and apparently arcing on the satellite surface. This interpretation of the observations is reinforced by the disappearance of the "arcing" signature (temporally narrow, wide frequency range pulses) when the neutralizer was turned on or when the beam accelerating voltage was switched off. The amplitude of the signals generated by these arcs were lower than those induced during natural charging events [*Koons et al.*, 1988; H.

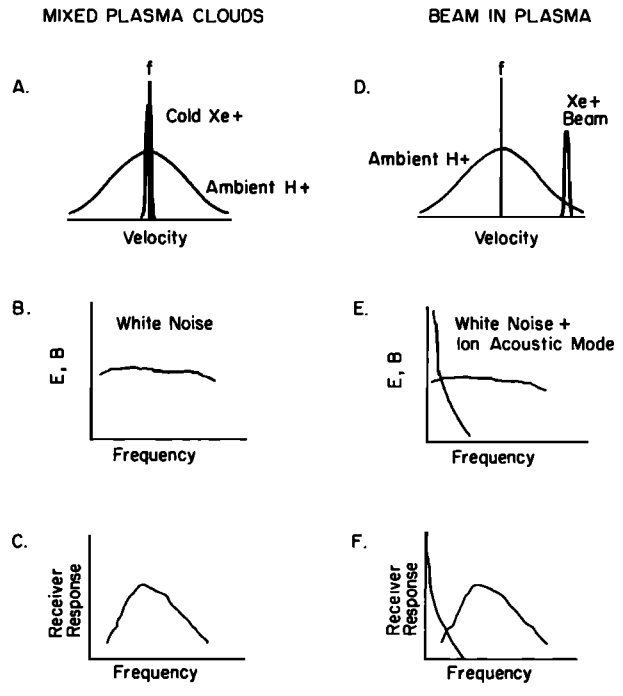

Fig. 12. Carton sketch of plasma conditions, plasma wave signals, and receiver response. (*a*) The curves are intended to represent Maxwellian distributions centered at $V = 0$. Parameters are; H^+: $n = 7$ cm^{-3}, $T = 5$ eV; Xe^+: $N = 0.002$ cm^{-3}, $T = 2$ eV. The extremely narrow distribution for the Xe^+ is due to the relatively high mass (131 amu). The Xe^+ density is artifically low in order to keep the central distribution on scale. A more realistic density for trickle mode is 10–100 cm^{-3}. (*b*) Both the electric (*E*) and magnetic (*B*) spectra are inferred to be relatively flat. (*c*) The receiver response is peaked in the 1–1.5 kHz frequency range. (*d*) The 1-keV xenon beam results in a "beam-like" distribution in the H^+ reference frame. Parameters are H^+: $n = 7.0$ cm^{-3}, $T = 5.0$ eV; Xe^+: $n = 0.0015$ cm^{-3}, $T = 2.0$ eV, $V = 38$ km/s. The xenon density in the beam would be orders of magnitude higher, and near the beam it might be more appropriate to consider the local H^+ to be a perturbation on the tail of the xenon distribution. (*e*) The white noise background is supplemented by an (inferred) ion-acoustic mode. (*f*) The receiver responds with a distribution peaked at low frequencies.

Koons, private communication, 1987]. These arcs did not generate pulses which were large enough to trigger the arc discharge monitor. The decrease in the arcing signature as the beam current was reduced (Figure 8) may be the result of changes in the gain (AGC) driven by the increase in the steady white noise spectrum or other beam-driven features.

The accelerated beam produced a distinct signal, in addition to the white noise background. This was the lower-frequency peak, most apparent in the electric antenna below 1 kHz. The two main cases are illustrated in Figure 12. For the non-accelerated beam (particularly trickle mode), Figure 12*a* shows the distribution function for the plasma near the satellite. Coincident with these (inferred) distributions, a white noise spectrum is generated by the discharge or the plasma distributions near the source, as sketched in Figure 12*b*. The receiver response (Figure 12*c*) is peaked at 1.0–1.5 kHz. The additional signal introduced by the (neutralized) beam is interpreted as the result of a beam in plasma distribution, as illustrated in Figure 12*d*. In addition to the combination of cold and hot plasmas, there is an offset in the beam center which may be sufficient to result in a positive slope distribution. Such distributions are unstable to waves such as the ion acoustic mode, which would have a frequency distribution similar to that shown in Figure 12*e* [*Chen*, 1984; *Kadmotstev*, 1965]. This would be combined with the white noise background, for the receiver response illustrated in Figure 12*f*.

The growth rate for instabilities such as the ion-acoustic mode depend upon basic parameters such as the beam temperature and density, relative to the ambient parameters. It is likely that both the "white noise" response of the receivers, and the response to the low-frequency beam produced modes can be explained by a detailed analysis of the appropriate beam-plasma dispersion relations. Such a treatment is substantially beyond the scope of the present work.

During trickle mode operations, the white noise signal is observed only on the magnetic antenna, which is physically close to the satellite. The electric antenna observes primarily natural signals. Examination of narrowband filter data for this mode shows that input to the electric field antenna at 30 kHz and below is at gun-off background levels, while the magnetic field antenna is still receiving signals with amplitude 20–30 dB above background. Hence, in general, trickle mode operations do not interfere with plasma wave observations on the long electric field antenna.

Trickle mode operations did produce two sets of signals unique to this mode. These were the 100-kHz signal seen in the electric antenna and the 20–200 Hz signal seen in the SC10 and SC11 data. The 100-kHz signal, seen only during the first example, would be consistent with electron plasma frequency, or upper hybrid resonance signals if the local plasma density is about 100 cm^3. This is a reasonable value, given a nominal trickle mode current of 40 μA, moving outward due to a positive spacecraft potential of a few volts, through a surface area of 10–100 m^2. The dimensions of the plasma cloud are comparable to the wavelength which might be expected for this frequency (e.g., 30 m for an index of refraction of 100). The lack of this feature in the second data set presented here could be due to fairly small variations in the plasma density, since the passband is fairly narrow (±7.5%). A variation in total electron density of 15% would move the signal out of the 100 kHz channel. Minor variations in gun performance could have this effect. Also, it is possible that variations in the nature of the ambient plasma could affect the amplitude of the signal, as with signals which are observed in the unperturbed plasmasphere [*Olsen et al.*, 1987].

The signal in the 20–200 Hz band is appropriate for ion (H^+) Bernstein waves, the lower hybrid resonance, or perhaps xenon (Xe^+) plasma waves. The ambient plasma is from the plasma sheet, with a normal density of 1 cm^3 and keV temperature. The ion composition of the plasma sheet is variable, but is primarily H^+, with 10–50% O^+. Hence the plasma environment around the satellite is primarily a Xe^+/electron plasma, with H^+ (or O^+) a minority constituent. If we assume a local density of 100 cm^{-3}, we obtain a xenon plasma frequency of ~180 Hz. If we use the measured magnetic field from the first event (80 γ), the lower hybrid resonance would be ~4 Hz for a xenon plasma, or ~50 Hz for an H^+ plasma. The gyrofrequencies are low, but ion Bernstein modes extend from f_{ci} to f_{LHR}. The most likely mode, from a frequency standpoint, is either the Xe^+ plasma wave, or H^+ Bernstein mode.

The spin modulation of the electric antenna data seen most

clearly in the second example (Figure 11) is similar to that found during observations of naturally occurring ion Bernstein waves (equatorial noise) with the same instrument [*Olsen*, 1981]. This indicates a dependence on magnetic aspect, which reflects wave polarization. The data from the magnetometer are taken from the axis parallel to the spin axis, and hence are not spin modulated.

The intense low-frequency (<100 Hz) signals normally found in the SC-1 electric antenna data (Figure 4*b*) disappeared during neutralized beam operations and some trickle mode operations. If this is not purely an AGC effect, it could be the result of shielding of the antenna from spacecraft generated noise. This would be analogous to the shielding of the DE 1 antenna from solar array noise observed in the plasmasphere [*Olsen et al.*, 1987].

3. CONCLUSIONS

The ion beam experiments on SCATHA produced a variety of plasma wave phenomenon. Arcing signatures were identified which can now be clearly associated with arcs on the satellite surface, not in the ion gun. This conclusion results from the disappearance of the arcing signature in trickle mode, when the full gas discharge is still operating, and the disappearance of the arcing signature when the beam is neutralized.

An intense white noise is generated near the satellite, which only couples weakly to the long electric antenna. This noise is largely independent of the gun mode. There is a lower-frequency signal which is observed only when an accelerated beam is emitted.

Trickle mode operations appeared to be relatively benign, in terms of interference with the natural plasma wave data. In fact, such operations offer the possibility of shielding plasma wave antenna from spacecraft generated signals. This is significant since this mode is close in its operational results to the behavior of a hollow cathode gas discharge, which is a primary design for future satellite potential control applications.

Acknowledgments. This work was supported by the Research Foundation at the Naval Postgraduate School, and the NASA Lewis Research Center. The work at the Aerospace Corporation was supported by the U.S. Air Force Systems Command's Space Division under contract F04701-88-C-0089. The authors would like to thank H. C. Koons, the principal investigator on the SC1 experiment, for providing the data, and for the use of processing facilities at Aerospace Corporation. We have profited from similar work done by D. Donatelli, at Air Force Geophysics Laboratory. The SC4 ion gun was operated by the PI, H. A. Cohen, and G. Mullin. The SC10 data were made available by T. L. Aggson, the SC11 data by B. G. Ledley, both at NASA/GSFC.

The Editor thanks K. Tsuruda and another referee for their assistance in evaluating this paper.

REFERENCES

Chen, F. F., *Introduction to Plasma Physics and Controlled Fusion*, 2nd ed., vol. 1, pp. 95–98, 267–273, Plenum, New York, 1984.

Erlandson, R. E., L. J. Cahill, C. J. Pollock, R. L. Arnoldy, W. A. Scales, and P. M. Kintner, Initial results from the operation of two argon ion generators in the ionosphere, *J. Geophys. Res.*, *92*, 4601–4616, 1987.

Fennell, J. F., Description of P78-2 (SCATHA) satellite and experiments, in *IMS Source Book*, pp. 65–78, AGU, Washington, D. C., 1982.

Haerendel, G., and R. Z. Sagdeev, Artificial Plasma Jet in the Ionosphere, Active Experiments in Space Plasmas, *Adv. Space Res.*, edited by C. T. Russell and M. J. Rycroft, *1*(2), 29–46, 1981.

Häusler, B., R. A. Treumann, O. H. Bauer, G. Haerendel, R. Bush, C. W. Carlson, B. Theile, M. C. Kelley, V. S. Dokukin, and Y. Y. Ruzhin, Observations of the artificially injected Porcupine xenon ion beam in the ionosphere, *J. Geophys. Res.*, *91*, 287–303, 1986.

Hudson, M. K., and I. Roth, Thermal fluctuations from an artificial ion beam injection into the ionosphere, *J. Geophys. Res.*, *89*, 9812–9822, 1984.

Hunter, R. E., R. O. Bartlett, R. M. Worlock, and E. L. James, Cesium contact ion microthruster experiments onboard Applications Technology Satellite (ATS)-IV, *J. Spacecr. Rockets*, *6*, 968–970, 1969.

Jones, D., Xe^+-induced ion-cyclotron harmonic waves, Active Experiments in Space Plasmas, edited by C. T. Russell and J. J. Rycroft, *Adv. Space Res.*, *1*(2), 103–106, 1981.

Kadomtsev, B. B., *Plasma Turbulence*, translated from Russian by L. C. Ronson, edited by M. G. Rusbridge, pp. 35–39, Academic, San Diego, Calif., 1965.

Kaufmann, R. L., D. N. Walker, J. C. Holmes, C. J. Pollock, R. L. Arnoldy, L. J. Cahill, and P. M. Kintner, Heavy ion beam–ionosphere interactions: Charging and neutralizing the payload, *J. Geophys. Res.*, *94*, 453–471, 1989.

Kerslake, W. R., and S. Domitz, Neutralization tests on the SERT II spacecraft, paper presented at 14th International Electric Propulsion Conference, Princeton Univ., Princeton, N. J., Oct. 30 to Nov. 1, 1979.

Kerslake, W. R., and R. C. Finke, SERT II spacecraft thruster restart—1974, *J. Spacecr. Rockets*, *12*, 780–782, 1975.

Kintner, P. M., and M. C. Kelley, Ion beam produced plasma waves observed by the $\Delta n/n$ plasma wave receiver during the Porcupine experiment, Active Experiments in Space Plasmas, edited by C. T. Russell and M. J. Rycroft, *Adv. Space Res.*, *1*(2), 107–115, 1981.

Kintner, P. M., and M. C. Kelley, Plasma waves produced by the xenon ion beam experiment on the Porcupine Sounding Rocket, in *Artificial Particle Beams in Space Plasma Studies*, edited by B. Grandal, pp. 199–205, Plenum, New York, 1982.

Kintner, P. M., and M. C. Kelley, A perpendicular ion beam instability: Solutions to the linear dispersion relation, *J. Geophys. Res.*, *88*, 357–359, 1983.

Koons, H. C., and H. A. Cohen, Plasma Waves and electrical discharges stimulated by beam operations on a high altitude satellite, in *Artificial Particle Beams in Space Plasma Studies*, edited by B. Grandal, pp. 111–120, Plenum, New York, 1982.

Koons, H. C., B. C. Edgar, J. F. Fennell, and D. J. Gorney, Observations of electron cyclotron harmonic emissions associated with field-aligned electron beams, *J. Geophys. Res.*, *92*, 7531–7537, 1987.

Koons, H. C., P. F. Mizera, J. L. Roeder, and J. F. Fennell, Severe spacecraft-charging event on SCATHA in September 1982, *J. Spacecr. Rockets*, *25*, 239–243, 1988.

Kudo, I., K. Machida, H. Murakami, and Y. Toda, Electromagnetic noise from an ion engine system, *J. Spacecr. Rockets*, *20*, 84–88, 1983.

Masek, T. D., and H. A. Cohen, Satellite positive-ion-beam system, *J. Spacecr. Rockets*, *15*, 27–33, 1978.

McPherson, D. A., and W. R. Schober, Spacecraft charging at high altitudes: The SCATHA satellite program, Spacecraft Charging by Magnetospheric Plasmas, edited by A. Rosen, *Progr. Aeronaut. Astronaut.*, *47*, 15–30, 1976.

McPherson, D. A., D. P. Cauffman, and W. Schober, Spacecraft charging at high altitudes—The SCATHA satellite program, paper presented at the 13th Aerospace Sciences Meeting, Am. Inst. of Aeronaut. Astronaut., Pasadena, Calif., 20–22, 1975.

Moore, T. E., R. L. Arnoldy, R. L. Kaufmann, L. J. Cahill, P. M. Kintner, and D. N. Walker, Anomalous auroral electron distributions due to an artificial ion beam in the ionosphere, *J. Geophys. Res.*, *87*, 7569–7579, 1982.

Olsen, R. C., Equatorially trapped plasma populations, *J. Geophys. Res.*, *86*, 11,235–11,245, 1981.

Olsen, R. C., Experiments in charge control at geosynchronous orbit—ATS-5 and ATS-6, *J. Spacecr. Rockets*, *22*, 254–264, 1985.

Olsen, R. C., S. D. Shawhan, D. L. Gallagher, J. L. Green, C. R. Chappell, and R. R. Anderson, Plasma observations at the Earth's magnetic equator, *J. Geophys. Res.*, *92*, 2385–2407, 1987.

Pottelette, R., J. M. Illiano, O. H. Bauer, and R. Treumann, Observation of high-frequency turbulence induced by an artificial ion beam in the ionosphere, *J. Geophys. Res.*, *89*, 2324–2334, 1984.

Roth, I., C. W. Carlson, M. K. Hudson, and R. L. Lysak, Simulations of beam excited minor species gyroharmonics in the Porcupine experiment, *J. Geophys. Res.*, *88*, 8115–8122, 1983.

Spitzer, L. Jr., *Physics of Fully Ionized Gases*, pp. 47–55, Wiley-Interscience, New York, 1956.

Thiel, J., L. R. O. Storey, O. H. Bauer, and D. Jones, Excitation of the lower oblique resonance by an artificial plasma jet in the ionosphere, *J. Geophys. Res.*, *89*, 2385–2387, 1984.

Walker, D. N., Perpendicular ion beam-driven instabililty in a multicomponent plasma: Effects of varying ion composition on linear flute mode oscillations, *J. Geophys. Res.*, *91*, 3305–3310, 1986.

Weddle, L. E., Ion gun generated electromagnetic interference on the SCATHA satellite, M.S. thesis, Nav. Postgrad. Sch., Monterey, Calif., 1987.

Werner, P., Ion gun operations at high altitudes, masters thesis, Nav. Postgrad. Sch., Monterey, Calif., 1988.

R. C. Olsen and L. E. Weddle, Physics Department PH-OS, Naval Postgraduate School, Monterey, CA 93943.

J. L. Roeder, Space Sciences Laboratory, Aerospace Corporation, M2-260, P.O. Box 92957, Los Angeles, CA 90009.

(Received March 28, 1989;
revised September 25, 1989;
accepted October 30, 1989.)